Communication in Physical Sciences, 2026, 13(2): 212-222

Analytical Study of the Thermoresistivity Behavior of Single-Walled (10,0) Zig-Zag Carbon Nanotube Using the Deng-Fan-Hulthen Potential Model

Ikechukwu Otete

Received: 23 November 2025/Accepted: 29 January 2026 /Published: 20 February 2026
https://dx.doi.org/10.4314/cps.v13i2.4

Abstract: *An analytical investigation of the thermoresistivity behavior of a semiconducting zig-zag single-walled (10,0) carbon nanotube is carried out using the Deng–Fan–Hulthén potential model. The Schrödinger wave equation is solved in the presence of magnetic and Aharonov-Bohm (AB) flux fields with the Nikiforov-Uvarov (NU) method to obtain the energy eigen value and wave function. With the energy equation, the partition function is calculated and used to evaluate the thermoresistivity properties of the nanotube in terms of temperature, tube's length and diameter. From the graphical plots, thermoresistivity of the carbon nanotube decreases with increasing temperature. As the nanotube length increases, the thermoresistivity decreases in value. With the tube's diameter, it is observed that the thermoresistivity also decreases as the diameter increases. The phonon-boundary and phonon-phonon scattering mechanism are responsible for this fundamental behavior.*

Keywords*: Deng-Fan-Hulthen Potential, Zig-Zag Single-Walled (10,0) Carbon Nanotube, Magnetic Field, Thermo Resistivity, Nikiforov-Uvarov method*

Ikechukwu Otete
Department of Physics, Federal University, Otuoke, Nigeria
Email: oteteii@fuotuoke.edu.ng

1.0 Introduction

Carbon nanotubes (CNTs) are among the most promising low-dimensional nanomaterials owing to their exceptional mechanical, electrical, and thermal properties, which make them suitable for advanced technological applications (Xiang *et al.,* 2025). Their nanoscale size and robust nature give them the ability to adapt to chemically hostile environments (Ado *et al*, 2008). CNTs are hollow cylindrical one-dimensional nanostructures composed of sp^2-hybridized carbon atoms arranged in a hexagonal lattice. (Mironov, 2017). CNTs are basically two types: the single-walled carbon nanotubes (SWCNTs) and the multi-walled carbon nanotubes (MWCNTs). Single-walled carbon nanotubes consist of a single rolled graphene sheet with diameters typically ranging from 0.4 to 10 nm and lengths extending to several micrometers, The multi-walled carbon nanotubes are made up of more than one layers of rolled-up graphene sheets in concentric forms that are kept bound by van der waal forces. Their diameter lies within few hundred nanometer range (Dhaval *et al.,* 2022)

Single-walled carbon nanotubes are either armchair, zig-zag or chiral nanotubes (Vajtai, 2013). Their metallicity is dependent on their chirality and diameter. Armchair SWCNTs (n,n) are metallic, whereas zig-zag (n,0) and chiral (n,m; $n \neq m \neq 0$) nanotubes may exhibit either semiconducting or metallic behavior depending on their chiral indices.. However, zig-zag single-walled carbon nanotubes can exhibit metallic features when n/3, (that is n is a multiple of 3) is an integer. Also, when (2n+m)/3 give an integer, chiral SWCNTs display the metallic features (Xu *et al.,* 2013; Erkan *et al.,* 2012). The chiral angle helps to determine the electronic properties of SWCNTs. In terms of the chiral vector$(\boldsymbol{C}_h)$ and chiral angle(θ), SWCNTs, structurally, can be formed into three types: zigzag, armchair and

chiral. In accordance to the different chiral angles, SWCNTs are grouped into zigzag ($\theta = 0^0$) armchair ($\theta = 30^0$) and chiral tubule ($0^0 < \theta < 30^0$). For armchair nanotubes, $n = m$ that is $\boldsymbol{C}_h = (n, n)$, zigzag nanotubes $m = 0$ that is $\boldsymbol{C}_h = (n, 0)$ and chiral nanotubes($n \neq m \neq 0$) whose mirror images have a different structure and different properties are displayed. Armchair nanotubes are metallic. Therefore, nanotubes possessing various forms of chirality (n, m) exhibit different physical, electronic, mechanical, optical, and thermal properties (Sebastien *et al.,* 2013; Lakhdar *et al.,* 2014; Mehrdad *et al.,* 2017; Ricardo, 2015).

According to Quan *et al.,* (2021), multi-walled carbon nanotubes can be metallic or semiconducting in nature. Using an AFMSEM-based micromanipulation robotic system, electrical contact between MWCNT bundles and different metal electrodes was made as reported in their experiment. A linear current-voltage characteristics curve shows that the MWCNT bundle is metallic, while a non-linear curve indicates that the MWCNT is semiconducting in nature (Yang *et al.,* 2021). The band structure of cylindrical nanotube is altered when the Aharonov-Bohm (AB) phase created around it in a magnetic field is parallel to its axis. A metallic CNT can be transformed into a semiconducting CNT and semiconducting tube can become metallic due to the effect of applied magnetic field. These field-induced modifications in band structure significantly influence the transport properties of CNTs, particularly their temperature-dependent electrical resistivity.–(Ado *et al.,* 2008; Ovchinnikov *et al.,* 1998).

Carbon nanotubes are reputed to exhibit high thermal conductivity, which has made them a much sought-after reinforcing agent for polymers and in the design of functional materials like thermal interface materials (TIMs) (George *et al*., 2020: & Singh, 2018).

In addition to the outstanding thermal properties of CNTs, their electrical and mechanical properties can be utilized in the design and construction of nano sensing elements like temperature, pressure, humidity, gas and electrochemical biosensors. Several theoretical and experimental studies have investigated the electrical and thermal transport properties of carbon nanotubes under varying external conditions. While experimental studies have reported temperature-dependent resistivity behavior in both metallic and semiconducting CNTs, most theoretical analyses are based on simplified potential models or tight-binding approximations. However, there remains limited analytical investigation of thermoresistivity behavior of specific chiral configurations such as the (10,0) zig-zag nanotube under combined magnetic and Aharonov–Bohm flux fields using more realistic molecular interaction potentials. These sensing elements can find application in the biomedical fields, security sectors, monitoring of the environment, automotive industry agricultural sector, manufacturing industries etc. In a cryogenic environment, accurate and precise temperature measurement is of utmost importance. And some of the temperature sensing devices available in research areas and cryogenic facilities are thermocouples, capacitors, transistor-based or resistor-based sensors. They are characterized with some drawbacks which include slow response time, low sensitivity and not cost-effective (Monea *et al.,* 2019). As the drum beat for miniaturization of electronics devices increases, CNTs, as nanomaterials, are seen as potential and viable candidates to replace silicon-based devices used as sensors. They are cost-effective, highly sensitive, low power consumption rate, quick response time and being able to adapt to areas prone to temperature fluctuations (Biabangard *et al.,* 2014; Monea *et al.,* 2019). Thus, CNTs being used as nano-sensors, detect signals at the atomic scale and transmit such signals to macroscopic level where such signals will be readily analyzed and interpreted (Zahraa, 2023). In the design of sensing devices, one of the electrical parameters of materials put into

consideration is their resistivity behavior. The resistivity of single-walled carbon nanotubes which is temperature dependent can occur due to some phenomenon like backscattering of electron of electrons and unklapp scattering (Kane *et al.,* 1998; Wallbank *et al.,* 2018). CNTs can exhibit a temperature-dependent resistivity when under the influence of thermal energy. This phenomenon is referred to as thermoresistivity of CNTs. Thermoresistivity refers to the response in terms of changes in temperature of the electrical resistance of a material. Materials or substances like metals have positive thermoresistivity. That is, the electrical resistance increases as the temperature increases. For single-walled carbon nanotubes that are semiconducting in nature, their thermo-resistivity is negative. That is, the electrical resistivity decreases with an increase in temperature. Metallic single-walled carbon nanotube has positive thermo-resistivity whose electrical resistivity increases with temperature increase (Francis, 2023). The thermoresistivity of CNTs is one of the thermodynamic properties obtained from the inverse or reciprocal of the thermal conductivity. CNTs' length, diameter and chirality are some of the structural parameters that could affect thermoresistivity (Qiang & Yanghua, 2014). A comprehensive theoretical understanding of thermoresistivity behavior is essential for optimizing CNT-based nanoelectronic and sensing devices, particularly in environments subjected to magnetic fields and temperature fluctuations. Analytical modeling provides predictive insight that complements experimental findings and guides device engineering.

Despite the extensive body of literature on CNT transport properties, there is a paucity of analytical studies that simultaneously incorporate external magnetic field effects, Aharonov–Bohm flux, and molecular interaction potentials such as the Deng–Fan–Hulthén potential in evaluating thermoresistivity behavior of semiconducting zig-zag nanotubes. This gap limits comprehensive understanding of field-modulated transport characteristics in low-dimensional systems. Therefore, this study presents an analytical investigation of the thermoresistivity behavior of a zig-zag single-walled (10,0) carbon nanotube using the Deng–Fan–Hulthén potential model. The resistivity characteristics are examined as functions of temperature, tube length, and diameter under the influence of external magnetic and Aharonov–Bohm flux fields. The analytical framework is developed through the solution of the Schrödinger wave equation using the Nikiforov–Uvarov method. This CNT has a symmetry group Pmmm, its length is 26.509 (Å), radius is 7.956(Å), and bond dissociation energy of 470.6KJ/mol (Constantino *et al*, 2019). It has a reported band gap of approximately 0.89 eV (Tetik, 2014).

This work is organized as follows: the Hamiltonian of a charged particle interacting with external magnetic field B and Ahanorov-Bohm (AB) flux within our confined potential where the SWE is solved analytically in the cylindrical coordinate with the NU method is in section 2. In section 3, the thermodynamic properties of resistivity is evaluated with the partition function. The results and discussion are contained in section 4 while the last section has the conclusion followed with the references.

1.1 Theoretical Framework

In cylindrical coordinates, the quantum Hamiltonian of a charged particle confined within the Deng–Fan–Hulthén potential under the combined influence of an external magnetic field BBB and an Aharonov–Bohm (AB) flux is written as equation 1

$$\frac{1}{2\mu}(i\hbar\vec{\nabla}-\frac{q}{c}\vec{A})^2+D_e\left(1-\frac{\delta}{(e^{\Lambda r}-1)}\right)^2-\frac{V_0e^{\Lambda r}}{(1-e^{-\Lambda r})}=E_{(n,m)}\psi_{(\rho,\varphi,z)} \quad (1)$$

where $\delta = e^{\Lambda r_e}$ -1, D_e represents the dissociation energy, r_e stands for the molecular bond length, r is the internuclear distance, Λ, is

the range of the potential well and V_o stands for the potential strength (Ikechukwu, 2026).

Here, μ, is the effective mass for a single-walled carbon nanotube. The summing of these two terms, $\vec{A} = \vec{A}_1 + \vec{A}_2$ make up the vector potential $\vec{A}$ and $\vec{\nabla} \times \vec{A}_1 = \vec{B}$ and $\vec{\nabla} \times \vec{A}_2 = 0$ is the symmetric or Coulomb gauge. B_z is the applied magnetic field along the z-direction. The additional magnetic flux Φ_{AB} is due to a solenoid. Thus, in the cylindrical coordinate system, the vector potential has the azimuthal components written as equation 2 (Ikechukwu, 2026):

$$\vec{A}_1 = \frac{\vec{B}e^{-\Lambda r}}{(1-e^{-\Lambda r})}, \ \vec{A}_2 = \frac{\Phi_{AB}}{2\pi r}\hat{\Phi} \text{ . So, } \vec{A} = \left(0, \frac{\vec{B}e^{-\Lambda r}}{(1-e^{-\Lambda r})} + \frac{\Phi_{AB}}{2\pi r}, 0\right) \quad (2)$$

The Deng-Fan-Hulthen Potential which is the potential model is of two different potentials-Deng-Fan and Hulthen potentials. Below is the graphical behavior of the potential model.

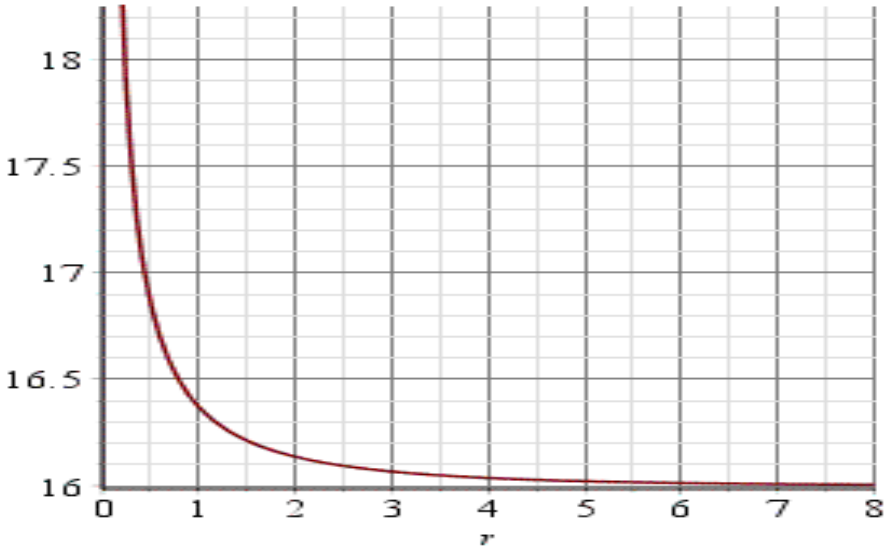

Fig. 1: Deng-Fan-Hulthen Potential graphical behavior

In the cylindrical coordinates our wave function is taken as:

$$\psi_{(r,\varphi)} = \frac{1}{\sqrt{2\pi}} e^{im\varphi} \ U_{nm,}(r) \ m = 0, \pm 1, \pm 2 \ldots \quad (3)$$

where m is the magnetic quantum number. By inserting the potential, vector potential, and the wave function into Eq. (1), a second-order differential equation written in Eq. (4) will be obtained:

$$\frac{d^2R_{nm}(r)}{dr^2} + \frac{2\mu}{\hbar^2}\left[E - D_e\left(1 - \frac{\delta}{(e^{\Lambda r}-1)}\right)^2 + \frac{V_o e^{-\Lambda r}}{(1-e^{-\Lambda r})} - \frac{2\hbar m e \Lambda \vec{B} e^{-\Lambda r}}{c(1-e^{-\Lambda r})} - \frac{e^2\vec{B}e^{-2\Lambda r}}{c^2(1-e^{-\Lambda r})^2} - \frac{e^2\vec{B}\Phi_{AB}e^{-\Lambda r}}{c^2(1-e^{-\Lambda r})^2 2\pi r} - \frac{((m+\xi)-\frac{1}{4})}{r^2}\right]R_{nm}(r) = 0 \quad (4)$$

The differential equation has both exponential and radial terms and the approximation scheme by Greene and Aldrich, written in equation 5 below, will help to solve the equation (Ikechukwu, 2026).

$$\frac{1}{r^2} \approx \Lambda^2\left[d_o + \frac{e^{-\Lambda r}}{(1-e^{-\Lambda r})^2}\right] \quad (5)$$

By inserting equation 5 into equation 6 we have

$$\frac{d^2R_{nm}(r)}{dr^2} + \left[\frac{2\mu E}{\hbar^2} - \frac{2\mu D_e}{\hbar^2} + \frac{4\mu D_e \delta e^{-\Lambda r}}{\hbar^2(1-e^{-\Lambda r})} \frac{2D_e\delta^2 e^{-2\Lambda r}}{\hbar^2(1-e^{-\Lambda r})^2} + \frac{2V_o e^{-\Lambda r}}{\hbar^2(1-e^{-\Lambda r})} - \frac{2m\eta\lambda\vec{B}e^{-\Lambda r}}{\hbar^2(1-e^{-\Lambda r})^2} - \frac{\eta^2\overrightarrow{B^2}e^{-2\Lambda r}}{\hbar^2(1-e^{-\Lambda r})^2} - \frac{\eta^2\Lambda\vec{B}\Phi_{AB}e^{-\Lambda r}}{\hbar^2(1-e^{-\Lambda r})^2\pi} - ((m+\xi)-\frac{1}{4})\Lambda^2\left(d_o + \frac{e^{-\Lambda r}}{(1-e^{-\Lambda r})^2}\right)\right]R_{nm}(r) = 0 \quad (6)$$

Where $\eta = \frac{e}{c}$, $\Phi_o = \frac{\hbar c}{e}$, $\xi = \frac{\Phi_{AB}}{\Phi_o}$ and $\delta = e^{\Lambda r} - 1$, c is the speed of light.

Using the transformation $z = e^{-\lambda r}$ (7)

After differentiating twice, you will obtain:

$$\frac{d^2}{dz^2} = \frac{\Lambda^2 z^2 d^2}{dz^2} + \frac{\Lambda^2 z d}{dz} \quad (8)$$

Substituting equation 8 into equation 6 and divide through by $\lambda^2 z^2$ the result will be:

$$\frac{d^2R_{nm}}{dz^2} + \frac{1}{z}\frac{dR_{nm}}{dz} + \frac{1}{z^2}\left[\frac{2\mu E}{\hbar^2\Lambda^2} - \frac{2\mu D_e}{\hbar^2\Lambda^2} + \frac{4\mu D_e \delta z}{\hbar^2\Lambda^2(1-z)} - \frac{2\mu D_e \delta^2 z^2}{\hbar^2\Lambda^2(1-z)^2} + \frac{2\mu V_o z}{\hbar^2\Lambda^2(1-z)} - \frac{2m\eta\vec{B}z}{\Lambda(1-z)^2} - \frac{\eta^2\vec{B}^2 z^2}{\hbar^2\Lambda(1-z)^2} - \frac{\eta^2\vec{B}\Phi_{AB}z}{\hbar^2\Lambda(1-z)^2\pi} - \left((m+\xi)^2 - \frac{1}{4}\right)\left(d_o + \frac{z}{(1-z)^2}\right)\right] R_{nm}(r) = 0 \quad (9)$$

We use the following dimensionless symbols for mathematical convenience

$$-\varepsilon = \frac{2\mu(E_{nm}-D_e)}{\hbar^2\Lambda^2},\ \alpha_1 = \frac{4\mu D_e\delta}{\hbar^2\Lambda^2},\ \alpha_2 = \frac{2\mu D_e\delta^2}{\hbar^2\Lambda^2},\ \gamma = \frac{2\mu V_o}{\hbar^2\Lambda^2}, \Sigma = \frac{2m\eta\vec{B}}{\hbar\Lambda}, \rho_1 = \frac{\eta^2\vec{B}^2}{\hbar^2\Lambda^2}, \rho_2 = \frac{\eta^2\vec{B}\Phi_{AB}}{\hbar^2\Lambda^2\pi}, V = \left((m+\xi)^2 - \frac{1}{4}\right) \quad (10)$$

Equation 9 can be rewritten with respect to these dimensionless symbols as:

$$\frac{d^2R_{nm}}{dz^2} + \frac{(1-z)}{z(1-z)}\frac{dR_{nm}}{dz} + \frac{1}{z^2(1-z)^2}[-\varepsilon(1-z)^2 + \alpha_1(1-z)z - \alpha_2(z^2) + \gamma(1-z)z - \Sigma(z) - \rho_1(z^2) - \rho_2(1-z)z - Vd_o(1-z)^2 - V(z)]\, R_{nm} = 0 \quad (11)$$

Subsequently, equation 11 can be evaluated further as:

$$\frac{d^2R_{nm}}{dz^2} + \frac{(1-z)}{z(1-z)}\frac{dR_{nm}}{dz} + \frac{1}{z^2(1-z)^2}[-(\varepsilon + \alpha_1 + \alpha_2 + \gamma + \rho_1 - \rho_2 + Vd_o)z^2 + (2\varepsilon + \alpha_1 + \gamma - \Sigma - \rho_2 + 2Vd_o - V)z - (\varepsilon + Vd_o)]\, R_{nm} = 0 \quad (12)$$

Equation 12 is compared with the parametric form of the NU of equation 13 12is written as (Otete and Eleje, 2023) :

$$R''_{(z)} + \frac{k_1 - k_2 z}{z(1-k_3 z)}R'_{(z)} + \left[\frac{-\zeta_1 z^2 + \zeta_2 z - \zeta_3}{z^2(1-k_3 z)^2}\right] R_{(z)} = 0 \quad (13)$$

The energy eigen values equation according to the NU is written as

$$k_2 n - (2n+1)k_5 + (2n+1)\left[\sqrt{k_9} + k_3\sqrt{k_8}\right] + n(n-1)k_3 + k_7 + 2k_3k_8 + 2\sqrt{k_8k_9} = 0 \quad (14)$$

The corresponding wave function is given as:

$$R_{nm}(z) = z^{k_{12}}(1 - k_3 z)^{-k_{12} - k_{13}/k_3}\, p_n^{k_{10}-1, \left(\frac{k_{11}}{k_3}\right) - (k_{10}-1)}(1 - 2k_3 z) \quad (15)$$

where the following parameters are written as

$$k_4 = \frac{1}{2}(1 - k_1) \quad (16)$$

$$k_5 = \frac{1}{2}(k_2 - 2k_3) \quad (17)$$

$$k_6 = k_5 + \zeta_1 \quad (18)$$

$$k_7 = 2k_4k_5 - \zeta_2 \quad (19)$$

$$k_8 = k^2{}_4 + \zeta_3 \quad (20)$$

$$k_9 = k_3k_7 + k^2{}_3k_8 + k_6 \quad (21$$

$$k_{10} = k_1 + 2k_4 + 2\sqrt{k_8} \quad (22)$$

$$k_{11} = k_2 - 2k_5 + 2(\sqrt{k_9} + k_3\sqrt{k_8}) \quad (23)$$

$$k_{12} = k_4 + \sqrt{k_8} \quad (24)$$

$$k_{13} = k_5 - (\sqrt{k_9} + k_3\sqrt{k_8}) \quad (25)$$

When equation 12 is compared with the parametric form of the NU of equation 13 the following, parameters can be found:

$$k_1 = k_2 = k_3 = 1 \quad (26)$$

$$\zeta_1 = \varepsilon + \alpha_1 + \alpha_2 + \gamma + \rho_1 - \rho_2 + \mathrm{V}d_o \quad (27)$$
$$\zeta_2 = 2\varepsilon + \alpha_1 + \gamma - \Sigma - \rho_2 + 2\mathrm{V}d_o - \mathrm{V} \quad (28)$$
$$\zeta_3 = \varepsilon + \mathrm{V}d_o \quad (29)$$

From equations 16 to 21, we obtain

$$\mathrm{k}_4 = \frac{1}{2}(1 - \mathrm{k}_1) = 0,\ \mathrm{k}_5 = \frac{1}{2}(\mathrm{k}_2 - 2\mathrm{k}_3) = -\frac{1}{2},\ \mathrm{k}_6 = \mathrm{k}_5^2 + \zeta_1 = \frac{1}{4} + \varepsilon + \alpha_1 + \alpha_2 + \gamma + \rho_1 - \rho_2 + \mathrm{V}d_o \quad (30)$$
$$\mathrm{k}_7 = 2\mathrm{k}_4\mathrm{k}_5 - \zeta_2 = -(2\varepsilon + k_1 + \gamma - \Sigma - \rho_2 + 2\mathrm{V}d_o - \mathrm{V}) \quad (31)$$
$$\mathrm{k}_8 = \mathrm{k}_4^2 + \zeta_3 = \varepsilon + \mathrm{V}d_o \quad (32)$$
$$\mathrm{k}_9 = \mathrm{k}_3\mathrm{k}_7 + \mathrm{k}_3^2\mathrm{k}_8 + \mathrm{k}_6 = \frac{1}{4} + \Sigma + \mathrm{V} + \rho_1 + \alpha_2 \quad (33)$$

In equation 10, it was shown that, $-\varepsilon = \frac{2\mu(E_{nm} - D_e)}{\hbar^2 \Lambda^2}$ (34)

Therefore, the substitution of equations 30 to 33 into equation 14, gave equation 35 after some algebra application, which finally represents the energy eigenvalue equation of the Deng-Fan-Hulthen potential is obtained as:

$$E_{nm} = -\frac{\hbar^2\Lambda^2}{2\mu}\left[\left(\frac{(\gamma - \lambda)}{2(\sigma + \sqrt{\gamma})} - \frac{(\sigma + \sqrt{\gamma})}{2}\right)^2 - \mathrm{V}d_o + D_e\right] \quad (35)$$

Where

$$\gamma = \frac{1}{4} + \Sigma + \mathrm{V} + \rho_1 + \alpha_2,\ \lambda = -\alpha_1 - \gamma + \Sigma + \rho_2 + \mathrm{V}, \sigma = n + \frac{1}{2} \quad (36)$$

Thus, equation 36 can be re-written in terms of the dimensionless symbols of Eq. (10) as:

$$\gamma = \frac{1}{4} + \frac{2m\eta\vec{B}}{\hbar\Lambda} + (m + \xi)^2 - \frac{1}{4} + \frac{\eta^2\vec{B}^2}{\hbar^2\Lambda^2} + \frac{2\mu D_e\delta^2}{\hbar^2\Lambda^2} \quad (37)$$
$$\lambda = -\frac{4\mu D_e\delta}{\hbar^2\Lambda^2} - \frac{2\mu V_o}{\hbar^2\Lambda^2} + \frac{2m\eta\vec{B}}{\hbar\Lambda} + \frac{\eta^2\vec{B}\Phi_{AB}}{\hbar^2\Lambda\pi} + (m + \xi)^2 - \frac{1}{4} \quad (38)$$

From Eqs. (22-25) we determine

$$\mathrm{k}_{10} = \mathrm{k}_1 + 2\mathrm{k}_4 + 2\sqrt{\mathrm{k}_8} = 1 + 2\sqrt{\varepsilon + \mathrm{V}d_0} \quad (39)$$
$$\mathrm{k}_{11} = \mathrm{k}_2 - 2\mathrm{k}_5 + 2(\sqrt{k + \mathrm{k}_3\mathrm{k}_8} = 2 + 2\left(\sqrt{\frac{1}{4} + \Sigma + \mathrm{V} + \rho_1 + \alpha_2 + \varepsilon + \mathrm{V}d_0}\right) \quad (40)$$
$$\mathrm{k}_{12} = \mathrm{k}_4 + \sqrt{\mathrm{k}_8} = \sqrt{\varepsilon + \mathrm{V}d_0} \quad (41)$$
$$\mathrm{k}_{13} = \mathrm{k}_5 - (\sqrt{\mathrm{k}_9} + \mathrm{k}_3\sqrt{\mathrm{k}_8}) = -\frac{1}{2} - \left(\sqrt{\frac{1}{4} + \Sigma + \mathrm{V} + \rho_1 + \alpha_2} + \sqrt{\varepsilon + \mathrm{V}d_0}\right) \quad (42)$$

Substituting Eqs. (39-42) into Eq. (15) the wave function written in Eq. (43) is obtained.

$$R_{nm}(\mathrm{z}) = \mathrm{z}^{\sqrt{\varepsilon + \mathrm{V}d_0}}(1 - \mathrm{z})^{\frac{1}{2} + \sqrt{\frac{1}{4} + \Sigma + \mathrm{V} + \rho_1 + \alpha_2}} P_n^{2\sqrt{\varepsilon + \mathrm{V}d_0},\, 2\sqrt{\frac{1}{4} + \Sigma + \mathrm{V} + \rho_1 + \alpha_2}}(1 - 2\mathrm{z}) \quad (43)$$

3. 0 The Partition Function and the Thermodynamic Properties of Carbon Nanotube

Thermal resistivity is one of the various thermodynamic properties of carbon nanotubes that can be determined. And to calculate this property, the partition function, which is temperature- dependent is evaluated first. At a particular temperature, when a direct summation is done over all possible energy levels, one can evaluate the partition function. It is written as (Otete, 2026):

$$Z(\beta) = \sum_n^{v_{max}} e^{-\beta E_{n,m}} \quad (44)$$

where $\beta = (K_B T)^{-1}$ with K_B as the Boltzmann constant, T, the temperature E_{nm} is the energy of the nth bound state where $n = 0, 1, 2, 3 \ldots, v_{max}$.

The energy eigen value of equation (35) can be re-written as:

$$E_{nm} = -\hbar^2\Lambda^2\left(\frac{N_1-(n+\gamma)^2}{2(n+\gamma)}\right)^2 + N_2 \qquad (45)$$

Where

$$N_1 = \frac{1}{4} + \frac{2m\eta\vec{B}}{\hbar\lambda} + (m+\xi)^2 - \frac{1}{4} + \frac{\eta^2\vec{B}^2}{\hbar^2\Lambda^2} + \frac{2\mu D_e\delta^2}{\hbar^2\Lambda^2} + \frac{4\mu D_e\delta}{\hbar^2\Lambda^2} - \frac{2\mu V_o}{\hbar^2\Lambda^2} + \frac{2m\eta\vec{B}}{\hbar\Lambda} + \frac{\eta^2\vec{B}\Phi_{AB}}{\hbar^2\Lambda\pi} + (m+\xi)^2 - \frac{1}{4} \qquad (46)$$

$$N_2 = \left((m+\xi)^2 - \frac{1}{4}\right) d_o\left(\frac{\hbar^2\Lambda^2}{2\mu}\right) + D_e \qquad (47)$$

Therefore, equation (44) can be recast as:

$$Z(\beta) = \sum_n^{v_{max}} e^{-\beta\left[-\frac{\hbar^2\Lambda^2}{2\mu}\left(\frac{N_1-(n+\gamma)^2}{2(n+\gamma)}\right)^2 + N_2\right]} \qquad (48)$$

The summation of equation (48) in the classical limit, is replaced by the integral. Thus, one have

$$Z_{(\beta)} = \int_0^v e^{\left(Dl^2\beta + \frac{H\beta}{l^2} + K\beta\right)} dl, l = n+\gamma \qquad (49)$$

Where

$$D = \frac{\hbar^2\Lambda^2}{8\mu}, H = -\frac{\hbar^2\Lambda^2N_1^2}{8\mu}, K = -\left(\frac{\hbar^2\Lambda^2N_1}{4\mu} + N_2\right) \qquad (50)$$

The Maple software is used to evaluate equation (49) to obtain the partition function of the system accosting2 to equation 31

$$\frac{1}{2}e^{D.\beta.l^2 + K.\beta\sqrt{H.\beta}}\left(\frac{2.v.e^{\frac{H.\beta}{v^2}}}{\sqrt{H.\beta}} - \frac{2\sqrt{H.\beta}\ \sqrt{\pi}\ erfi\left(\frac{H.\beta}{v}\right)}{\sqrt{H.\beta}} - 2\sqrt{\pi}\right) \qquad (51)$$

where erfi(k) denotes the imaginary error function (Otete, 2026) define according to equation 52

$$\text{erfi}(k) = ierf(k) = \frac{2}{\sqrt{\pi}}\int_0^k e^{t^2}dt \qquad (52)$$

In Maple software, this error function is used for various numerical calculations.

With the partition function of the system known, the thermal resistivity is gotten from the reciprocal of thermal conductivity denoted K, which is a function of heat capacity, phonon group velocity and the free mean path. The thermal conductivity of carbon nanotubes is written as (Michael *et al.,* 2009):

$$K = \frac{1}{3}\rho c v^2\tau_s \qquad (53)$$

Here, c, v, and τ represent specific heat per unit volume, group velocity and relaxation time or free mean path of a given phonon state, respectively (Bounphanh, 2011). The specific heat capacity is given by the relation (Khordad *et al*., 2017)

$$C_v = = \frac{\partial U}{\partial T} = k_B\beta^2\frac{\partial^2 lnZ}{\partial\beta^2} \qquad (54)$$

So we can write the thermal conductivity as equation 35

$$K = \frac{1}{3}\rho v^2\tau_s k_B\beta^2\frac{\partial^2 lnZ}{\partial\beta^2} \qquad (55)$$

So the inverse of the expression written in Eq. (55) will give the thermal resistivity. Its unit is K.m/w.

The graphical plots of the resistivity with temperature variation and bond length and diameter in Figs, 2,3 and 4.

4.0 Results and Discussion

Traditionally, the resistivity of pure conductors or metals decreases with decreasing temperature because the scattering effect of the charge during transportation is less. But for semiconductors, their resistivity decreases as the temperature increases. This is as a result of the increased number of the charge carriers and their mobility which are excited thermally by the rise in temperature (Agnieszka *et al.,* 2014). Thus, in Fig. 2, the thermoresistivity of the zig-zag single-walled (10, 0) carbon nanotube is seen to decrease as the temperature rises. The

plot of thermoresistivity versus tube length is shown in Fig. 3.

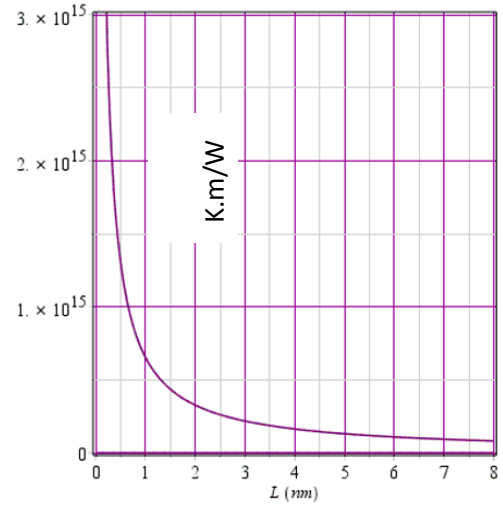

Fig. 3: Plot of thermal resistivity versus tube's length

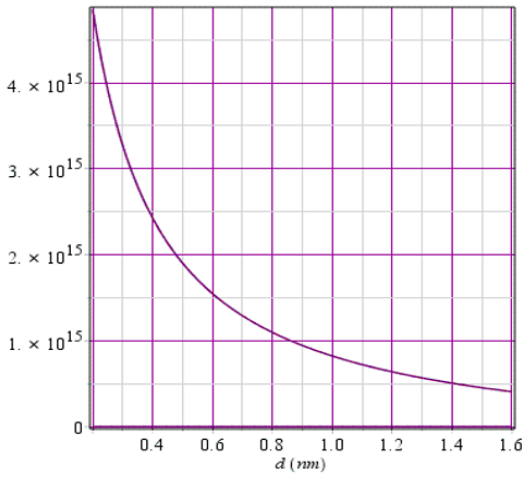

Fig. 4: Plot of thermal resistivity versus tube's diameter

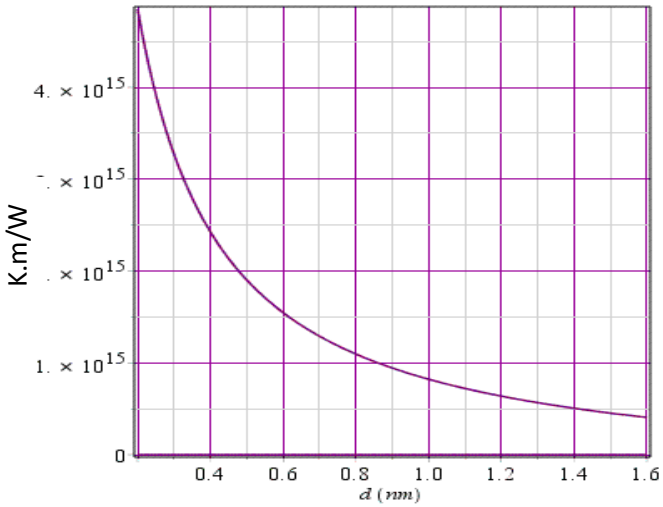

Fig. 4: Plot of thermal resistivity versus tube's diameter

It is seen that the thermoresistivity decreases as the carbon nanotube length increases. In semiconducting CNTs, phonons are the medium or channels heat is transported. As the carbon nanotube length increases, the barrier caused by phonon-phonon scattering to the ballistic movement of phonons through the CNT becomes less dominant. This necessitate an increase in the thermal transport that varies proportionally to the tube's length. Thus, there is an increase in the thermal conductivity, which implies low resistivity (Leonard *et al.,* 2017). In Fig, 4, the plot of thermoresistivity versus tube diameter is shown. As could be seen, the thermoresistivity decreases as the carbon nanotube diameter is increasing. This behavior is attributed to the fact that as the diameter increases, the curvature effects are reduced and more phonon modes dispersion relations tend close to those of planar graphene.

Therefore a more scattered phonon mode participating in thermal conduction or transportation due to higher phonon group velocities are necessitated. This leads to a lower thermoresistivity value (Hone, 2001).

5. 0 Conclusion

By using the Deng-Fan-Hulthen potential model, the thermoresistivity nature of zig-zag (10,0) carbon nanotube was investigated by solving the Schrödinger wave equation using the NU method. The energy eigen value equation and the wave function were obtained analytically and with the energy eigen value equation, the partition function was calculated. The thermodynamic property of thermoresistivity as a function of temperature, tube's length and diameter was evaluated with the help of Maple software. From the results of the graphical plots, it was observed that increasing the temperature of the CNT causes the thermoresistivity to decrease. For the tube's length and diameter, the thermoresistivity decreases as the tube's length and diameter increase. This behavior of this CNT shows its semiconducting nature. This property of carbon nanotubes could serve as a finger print in the design and construction of diversified nanoelectronic sensors that will be useful in nanotechnology.

4.0 References

Ado, J., Gene, D., & Mildred, S. D. (Eds.). (2008). *Carbon nanotubes: Advanced topics in the synthesis, structure, properties and applications*. Springer-Verlag, Berlin Heidelberg.

Agnieszka, L.-R., Jeff, P., Lukasz, K., John, B., & Krzytof, K. (2014). Electrical properties of carbon nanotube based fibers and their future use in electrical wiring. *Advanced Functional Materials*, 24, pp. 3661–3682. https://doi.org/10.1002/adm.201303716

Amirrhossein, B. O., Uttandaramam, S., & Pierre, M. (2014). Effect of temperature on electrical resistivity of carbon nanotubes and graphene nanoplatelets nanocomposites. *Journal of Nanotechnology in Engineering and Medicine*, 5, pp. 044501-1–044501-6. https://doi.org/10.1115/1.4030018

Bo, X., Jiang, Y., & Zhiguo, L. (2013). Phonon scattering and electron transport in single wall carbon nanotubes. https://dx.doi.org/10.5772/51451

Bogdan, F. M., Eusebiu, L. I., Stefan, I. S., Daniela, I.-E., & Emil, P. (2019). Carbon nanotubes structures used for temperature measurement. *Sensors*, 19, pp. 2464–2475. https://doi.org/10.3390/s19112464

Bounphanh, T. (2011). *Thermal and mechanical studies of carbon nanotube polymer composites synthesized at high pressure and high temperature*. Doctoral thesis, Department of Physics, University of Umea, Sweden.

Constantinos, O., Zeinalipour-Yazdi, E., Loizidou, Z., & Arunabhiram, C. (2019). Size-dependent bond dissociation enthalpies in single-walled carbon nanotubes. *Chemical Physics Letters*, 731, pp. 136628–136635. https://doi.org/10.1016/ .cplett.2019.136628

Dhaval, A., Vartak, Y., Ghotekar, P. B., Bharat, M. H. S., Vadher, J. A., & Munjal, B. S. (2022). Carbon nanotube composites to enhance thermal and electrical properties for space applications: A review. *Journal of Environmental Nanotechnology*, 11, 3, pp. 1–12. https://doi.org/10.13074/jent.2022n.09.223456

Eddy, N. O., Odiongenyi, A. O., Garg, R., Ukpe, R. A., El Nemir, A., Ngwu, C. M., & Okop, I. J. (2023). Quantum and experimental investigation of the application of *Crassostrea gasar* (mangrove oyster) shell based CaO nanoparticles as adsorbent and photocatalyst for the removal of procaine penicillin from aqueous solution. *Environmental Science and Pollution Research*. https://doi.org/10.1007/s11356-023-26868-8

Erkan, T. (2014). The electronic properties of doped single walled carbon nanotubes and carbon nanotubes sensors. *Condensed Matter Physics*, 17, 4, pp. 1–12. https://doi.org/10.5488/CMP.17.43301

Erkan, T., Faruk, K., Muharrem, K., & Ibrahim, C. (2012). The electronic properties of graphene and carbon nanotubes: Ab initio density functional theory investigation. *ISRN Nanotechnology*, 2012, pp. 1–10. https://doi.org/10.5402/2012/416417

Eshghi, M., & Mehraban, H. (2017). Study of a 2D charged particle confined by a magnetic and AB flux fields under the radial scalar power potential. *European Physical Journal Plus*, 132, pp. 121–129. https://doi.org/10.1140/epjp/i2017-11379-x

Francis, A. (2023). Thermoresistivity of carbon nanostructures and their polymeric nanocomposites. *Advanced Materials Interfaces*, 10, 31, pp. 2300218–2300225. https://doi.org/10.1002/admi.202300218

George, T., Georgia, T., Vitaly, D., Labrini, S., Asterios, B., Dimitrios, T., John, P., Christoforos, K., Stavroula, G., Costas, G., & Kostas, P. (2020). Mechanical, electrical, and thermal properties of carbon nanotube buckypapers/epoxy nanocomposites produced by oxidized and epoxidized nanotubes. *Materials*, 13, pp. 4308–4319. https://doi.org/10.3390/ma13194308

Hone, J. (2001). Phonons and thermal properties of carbon nanotubes. In *Topics in Applied Physics* (Vol. 80). Springer.

Kanchan, K., & Singh, D. N. (2018). A relation between thermal conductivity and specific heat capacity of CNT. *International Journal of Advanced Research in Engineering and Technology*, 9, 4, pp. 208–213.

Kane, C. L., Mele, E. J., Lee, R. S., Fisher, J. E., Petit, P., Dai, H., Thess, A., Smalley, R. E., Verschueren, A. R. M., Tans, S. J., & Dekker, C. (1998). Temperature dependent resistivity of single wall carbon nanotubes. *Europhysics Letters*, 41, 6, pp. 683–688.

Khordad, R., & Rastegar Sedehi, H. R. (2017). Thermodynamic properties of a double ring-shaped quantum at low and high temperatures. *Journal of Low Temperature Physics*, pp. 1–10. https://doi.org/10.1007/s10909-017-1831-x

Lakhdar, B., Mohamed, Z., Abdelnour, B., & Abdelouahed, T. (2014). A Timoshenko beam model for vibration analysis of chiral single-walled carbon nanotubes. *Physica E*, 59, pp. 180–191.

Wu, M. C. H., & Jang-Yu, H. (2009). Thermal conductivity of carbon nanotubes with quantum correction via heat capacity. *Nanotechnology*, 20, pp. 145401–145406. https://doi.org/10.1088/0957-4484/20/14/145401

Mironov, G. I. (2017). The energy spectrum of zig-zag single-walled carbon nanotubes in the Hubbard model in the static fluctuation approximation. *Low Temperature Physics*, 43, 6, pp. 1–7. https://doi.org/10.1063/1.4985980

Ogoko, E. C., Kelle, H. I., Akintola, O., & Eddy, N. O. (2023a). Experimental and theoretical investigation of *Crassostrea gigas* shells based CaO nanoparticles as a photocatalyst for the degradation of bromocresol green dye (BCGD) in an aqueous solution. *Biomass Conversion and Biorefinery*. https://doi.org/10.1007/s13399-023-03742-8

Otete, I., & Eleje, C. B. (2023). Magnetic field effect on the energy spectra of InP quantum dot in D-dimensions with Hulthen-Yukawa potential. *Asian Research Journal of Current Science*, 5, 1, pp. 20–27.

Declaration

Consent for publication

Not Applicable

Availability of data and materials

The publisher has the right to make the data public

Conflict of Interest
The authors declared no conflict of interest
Ethical Considerations
Not applicable
Competing interest
The authors report no conflict or competing interest

Funding
The author declared no source of funding
Author Contributions
All components of the work were carried out ny the author